

9-15-2022

A Novel Self-Assembled Cobalt-Free Perovskite Composite Cathode with Triple-Conduction for Intermediate Proton-Conducting Solid Oxide Fuel Cells

Hua Tong

Min Fu

Yang Yang

Fanglin Chen

University of South Carolina - Columbia, chenfa@cec.sc.edu

Zetian Tao

Follow this and additional works at: https://scholarcommons.sc.edu/emec_facpub



Part of the [Mechanical Engineering Commons](#)

Publication Info

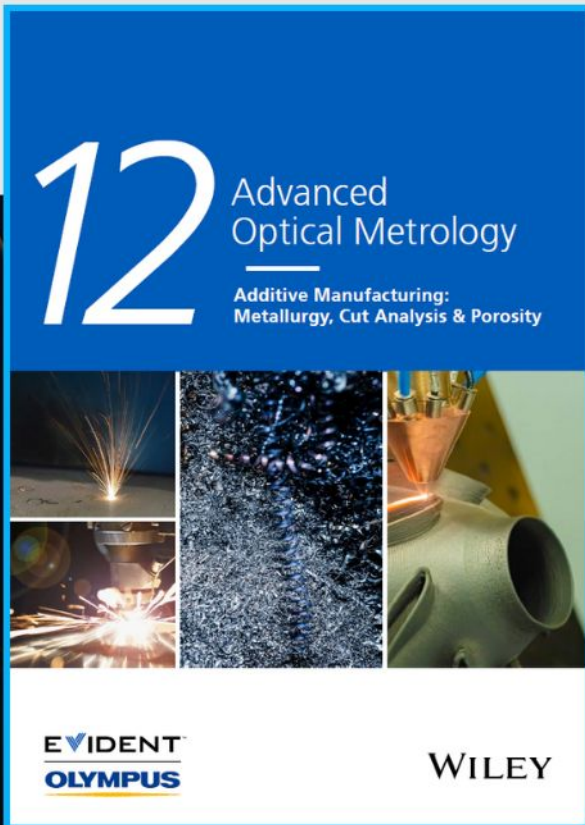
Published in *Advanced Functional Materials*, 2022.

© 2022 The Authors. *Advanced Functional Materials* published by Wiley-VCH GmbH. This is an open access article under the terms of the [Creative Commons Attribution License](#), which permits use, distribution and reproduction in any medium, provided the original work is properly cited.

This Article is brought to you by the Mechanical Engineering, Department of at Scholar Commons. It has been accepted for inclusion in Faculty Publications by an authorized administrator of Scholar Commons. For more information, please contact digres@mailbox.sc.edu.



Additive Manufacturing: Metallurgy, Cut Analysis & Porosity



The latest eBook from
Advanced Optical Metrology.
Download for free.

In industry, sector after sector is moving away from conventional production methods to additive manufacturing, a technology that has been recommended for substantial research investment.

Download the latest eBook to read about the applications, trends, opportunities, and challenges around this process, and how it has been adapted to different industrial sectors.

EVIDENT™
OLYMPUS

WILEY

A Novel Self-Assembled Cobalt-Free Perovskite Composite Cathode with Triple-Conduction for Intermediate Proton-Conducting Solid Oxide Fuel Cells

Hua Tong, Min Fu, Yang Yang, Fanglin Chen,* and Zetian Tao*

A traditional composite cathode for proton-conducting solid oxide fuel cells (H-SOFCs) is typically obtained by mixing cathode materials and proton conducting electrolyte of $\text{BaCe}_{0.7}\text{Y}_{0.2}\text{Zr}_{0.1}\text{O}_{3-\delta}$ (BZCY), providing chemical and thermal compatibility with the electrolyte. Here, a series of triple-conducting and cobalt-free iron-based perovskites as cathodes for H-SOFCs is reported. Specifically, $\text{BaCe}_x\text{Fe}_{1-x}\text{O}_{3-\delta}$ ($x = 0.36, 0.43, \text{ and } 0.50$) shows various contents of two single phase perovskites with an in situ heterojunction structure as well as triple conductivity by tailoring the Ce/Fe ratios. The cell performance with the optimized $\text{BaCe}_{0.36}\text{Fe}_{0.64}\text{O}_{3-\delta}$ (BCF36) cathode composition reaches 1056 mW cm^{-2} at 700°C . Moreover, a record cell performance of 1525 mW cm^{-2} at 700°C is obtained by modifying the BCF36 cathode microstructure through a spraying method, demonstrating high promise with Co-free cathodes for H-SOFCs.

1. Introduction

Owing to the urgent demands of clean energy and environmental protection, proton-conducting solid oxide fuel cells (H-SOFCs) have attracted much attention in the past several decades due to their promising cell performance and high energy conversion efficiency at intermediate temperatures.^[1–4] Proton conductors such as $\text{BaCe}_{0.7}\text{Zr}_{0.1}\text{Y}_{0.2}\text{O}_3$ (BZCY) have high mobility of protons and are perceived as ideal electrolytes for H-SOFC due to their high proton conductivity and chemical stability under cell operation conditions.^[5,6]

Nevertheless, reducing the operating temperature is still a big challenge because the cathode materials without high electrochemical catalytic activity sensitively affect cell performance with

the decrease in the cell operating temperatures. Cathode reactions such as oxygen reduction reaction, oxygen ion diffusion, and proton migration are significantly influenced by the operating temperatures.^[7] In previous studies, $\text{La}_{0.6}\text{Sr}_{0.4}\text{Co}_{0.2}\text{Fe}_{0.8}\text{O}_{3-\delta}$ (LSCF), $\text{Ba}_{0.5}\text{Sr}_{0.5}\text{Co}_{0.8}\text{Fe}_{0.2}\text{O}_{3-\delta}$ (BSCF), $\text{BaCo}_{0.4}\text{Fe}_{0.4}\text{Zr}_{0.1}\text{Y}_{0.1}\text{O}_{3-\delta}$ (BCFZY), and other cobalt-based oxides with mixed conductivity of oxygen ion and electron are reported as cathodes for H-SOFCs, presenting excellent catalytic activity for oxygen reduction reaction (ORR) at intermediate operation temperature.^[8–13] However, these cathodes often suffer from some drawbacks such as high thermal expansion coefficients (TECs) and easy

evaporation of cobalt at high temperature.^[14] Moreover, considering the basic cathode reactions of H-SOFCs, triple conductivity of proton, oxygen ion and electron are effective to extend catalytic active sites.^[14–16] Thus, introducing proton conductivity to the cathode materials is of significant importance to develop proper cathodes for H-SOFCs.^[17]


Historically, proton-conducting electrolyte has been mixed with cathode materials to form composite cathodes for H-SOFCs.^[3,11,12,18,19] It has been reported that the composite cathode not only increases the cathode reaction rate, but also adjusts the TEC of the cathode to satisfy thermal compatibility requirements. Later on, single-phase perovskite oxides capable of simultaneously transporting proton, oxygen ion, and electronic defects have been developed for H-SOFCs, leading to superior ORR activity.^[16,20–22]

Single phase BaFeO_3 (BFO) has been evaluated as cathode material for H-SOFCs.^[23,24] Doped barium cerates have also been investigated as cathode materials due to their high thermal and chemical compatibility with the electrolyte. Furthermore, Fe-doped BaCeO_3 (BCO) shows intrinsic triple-conducting behavior, which can extend the electrochemical reaction sites to the entire electrode surface,^[25] and is beneficial to the cell performance.^[21] In addition, self-assembled composite cathode consisting of double perovskite and single perovskite oxide phases has been reported to enable a stable high electrochemical activity through the synergic integration of the distinct properties.^[26,27] The objective of this study is to evaluate Fe-doped BaCeO_3 with self-assembled two single phase perovskites with in situ heterojunction structure as Co-free composite cathode for H-SOFCs.

Nominal $\text{BaCe}_x\text{Fe}_{1-x}\text{O}_{3-\delta}$ ($x = 0.36, 0.43, \text{ and } 0.50$) powders comprising cubic perovskite (CP) and orthorhombic perovskite

H. Tong, M. Fu, Y. Yang, Z. Tao
School of Resources, Environment and Safety Engineering
University of South China
Hengyang, Hunan Province 421001, China
E-mail: newton@mail.usc.edu.cn, taozetian@usc.edu.cn

F. Chen
Department of Mechanical Engineering
University of South Carolina
Columbia, SC 29208, USA
E-mail: chenfa@cec.sc.edu

 The ORCID identification number(s) for the author(s) of this article can be found under <https://doi.org/10.1002/adfm.202209695>.

© 2022 The Authors. Advanced Functional Materials published by Wiley-VCH GmbH. This is an open access article under the terms of the Creative Commons Attribution License, which permits use, distribution and reproduction in any medium, provided the original work is properly cited.

DOI: 10.1002/adfm.202209695

(OP) structure are self-assembled through an in situ sol-gel method. The intrinsic triple conducting behavior is optimized by tailoring the Ce/Fe ratios, and $\text{BaCe}_{0.36}\text{Fe}_{0.64}\text{O}_{3-\delta}$ (BCF36) exhibits excellent ORR activity as well as oxygen ion transport capacity. Furthermore, single cells with spray-coated BCF36 cathode display the highest maximum power density of 1525 mW cm^{-2} at $700 \text{ }^\circ\text{C}$ compared with other cobalt-free cathodes, presenting a promising strategy to design triple conducting cathodes for H-SOFCs.

2. Results and Discussion

XRD patterns of the BCF series of oxide powders shown in Figure S1 (Supporting Information) indicate that all powders are successfully synthesized with no detectable impurities. The characteristic diffraction patterns show that all samples comprise two different types of perovskite oxides: cubic perovskite (CP) and orthorhombic perovskite (OP) structures.^[21] The CP phase BFO possesses high oxygen ion permeability and electron conductivity^[23] while the OP phase BCO is a good proton conductor. The self-assembled CP/OP mixture may have respective conducting property to obtain triple conducting behavior that is beneficial for lowering ASR values.^[28] Rietveld refinement of XRD patterns for BCF36 in Figure 1a display that the crystal structures consist CP phase (74.39 wt.%) and OP phase (25.60 wt.%) with a reasonable reliability fitting factor of 1.35. In term of $\text{BaCe}_{0.5}\text{Fe}_{0.5}\text{O}_{3-\delta}$ (BCF50), XRD refinement in Figure 1b reveals the composition is CP phase (50.9 wt.%) and OP phase (49.05 wt.%). Thus, the CP/OP composition is regulated by tailoring the Ce/Fe amounts that may change conducting behavior and affect cathode reaction process through synergistic effect between the two CP/OP phases.^[26]

Figure 2 is the high-resolution TEM images of BCF36 powders after heat-treated at $1000 \text{ }^\circ\text{C}$. As shown in Figure 2b, lattice fringe spacing distances of 0.378 and 0.301 nm correspond to the (100) facets of BFO and (110) facets of BCO, respectively, suggesting that BFO and BCO phases co-exist and are uniformly distributed in the BCF36 powders. Moreover, the dispersibility of the multi-phases is further established by

the X-ray energy dispersive spectrum mapping of Ba, Ce, and Fe, indicating that all elements are distributed homogeneously with no observable elemental segregation.

Electrical conductivity relaxation (ECR) technique is employed to study kinetic properties of the BCF materials (Figure S2, Supporting Information). The horizontal axis represents relaxation time from initial equilibrium to a new equilibrium after the oxygen partial pressure surrounding the sample was changed from 0.21 to 0.5 atm. The normalized electrical conductivity of BCF36 and BCF50 at various temperatures is fitted according to the pure surface-controlled equilibration kinetics^[29] and the results are summarized in Table S1 (Supporting Information). Oxygen surface exchange coefficients (K_{ef}) and diffusion coefficients (D_{ef}) are $5 \times 10^{-3} \text{ cm s}^{-1}$ and $3 \times 10^{-4} \text{ cm}^2 \text{ s}^{-1}$ for BCF36 at $700 \text{ }^\circ\text{C}$, while those are $6 \times 10^{-3} \text{ cm s}^{-1}$ and $1.5 \times 10^{-4} \text{ cm}^2 \text{ s}^{-1}$ for BCF50 at $700 \text{ }^\circ\text{C}$, respectively. K_{ef} represents the rate of oxygen adsorption and dissociation while D_{ef} is deemed as a key factor of oxygen ion diffusion inside the cathode. The values of K_{ef} and D_{ef} are crucial to reduce the polarization resistance of the cathode,^[30] indicating that BCF36 has a better electrochemical performance from the point of view of oxygen ion transmission. In addition, the higher electronic conductivity of BCF36 for the high percentage of CP phase is beneficial for the charge transfer process and the conductivity values at intermediate temperatures are sufficient for use as cathodes for SOFCs (Figure S3, Supporting Information).^[14,31] In order to clarify the detailed chemical states of BCF series powders, XPS analysis of O1s, Fe, and Ce has been conducted with the results presented in Figure S4 (Supporting Information). It can be seen that the proportion of adsorbed oxygen increases while Fe^{4+} decreases from BCF50 to BCF36, suggesting the ORR activity might be enhanced that is consistent with the ECR results.^[32]

To further demonstrate the influence of Ce/Fe amounts on electrochemical performance, anode-supported SOFCs with BCF cathodes are tested at $700 \text{ }^\circ\text{C}$. As shown in Figure 3a, maximum power densities (MPDs) of 1056, 885, and 558 mW cm^{-2} are achieved for BCF36, BCF43, and BCF50, respectively. BCF 36 shows the best performance among these three different cathodes, indicating that triple conducting

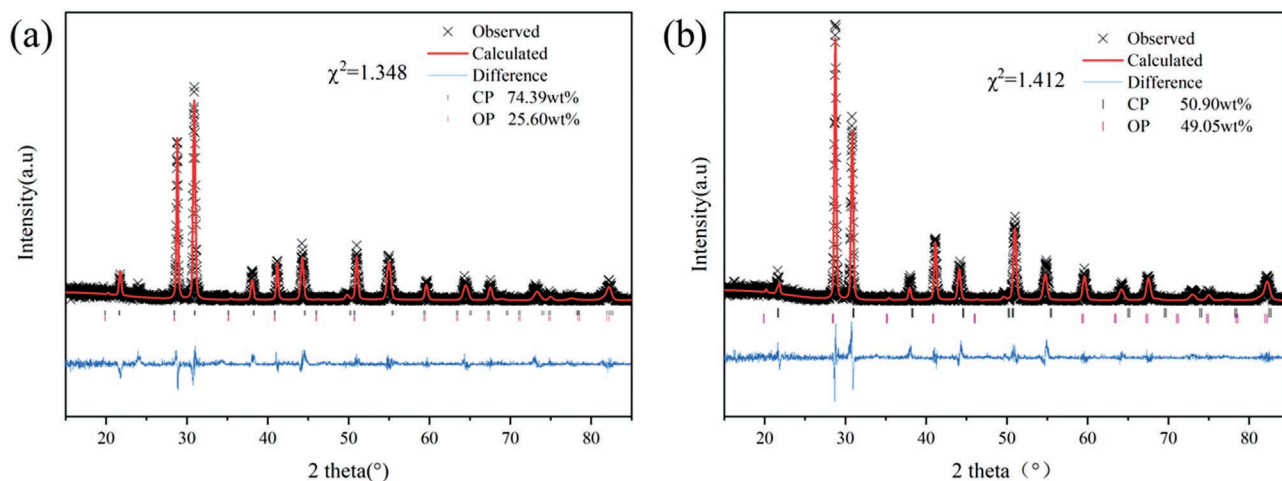


Figure 1. a) Refined XRD profiles of BCF36 sample and b) BCF50 sample.

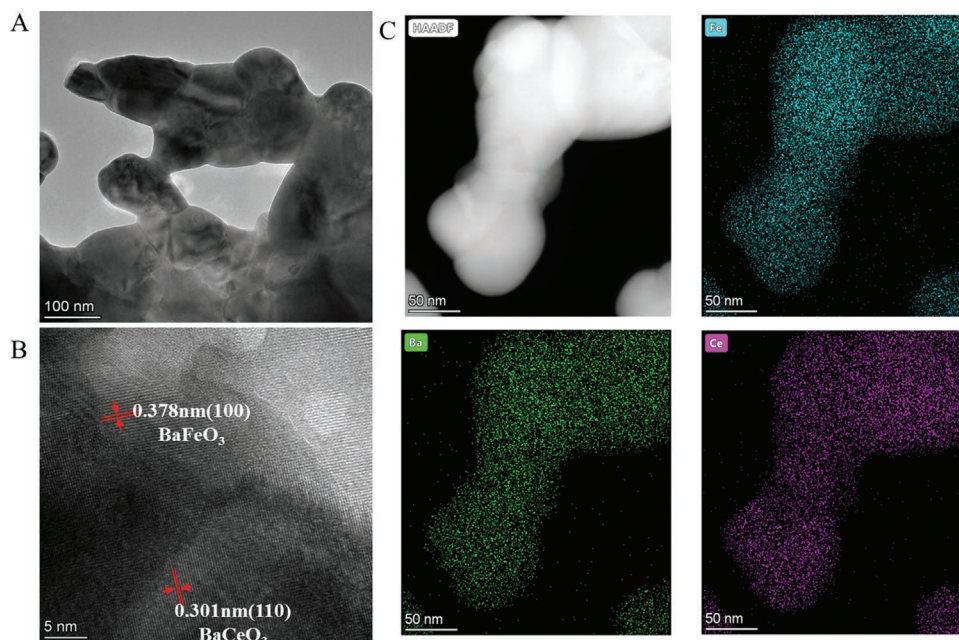


Figure 2. Transmission electron microscopy (TEM) analysis of BCF36 nanoparticle and corresponding energy-dispersive X-ray spectroscopy (EDS) maps of Ba, Fe, and Ce.

capacity is well balanced for BCF36. Moreover, the durability of the single cell at 600 °C with an applied voltage of 0.6 V has been evaluated and shown in Figure 3b. As it can be seen in Figure 3b, the current is stable for 100 h without any obvious degradation, demonstrating that the composite cathode of BCF36 has an excellent chemical capability to moisture and CO₂ in the ambient air.

The impedance spectra of single cells using BCF series cathodes under open circuit voltage (OCV) condition are tested to evaluate the cathode reaction processes (Figures S5–S10, Supporting Information). The high frequency intercept of the impedance spectra corresponds to the ohmic resistance that is directly related to the thickness of the electrolyte. The cross-sectional images of the single cells (Figure S11, Supporting

Information) indicate that the cells with different cathode compositions have similar electrolyte thickness and morphology, expecting to have little impact on the ohmic resistance. The difference between the high frequency and low frequency intercepts with the real axis represents the total interfacial polarization resistance (R_p) of the cell. There are at least two rate limiting steps such as charge transfer and ion diffusion on the surface of the cathode.^[33] To clearly observe the difference, the polarization resistances at various temperatures are plotted in Figure 4a; R_p of BCF36 is $\approx 0.060 \Omega \text{ cm}^2$ at 700 °C, which is clearly smaller compared to the other two cells. In order to elucidate the cathode processes, distribution of relaxation time (DRT) is applied to analyze the impedance spectra at 700 °C.^[34,35]

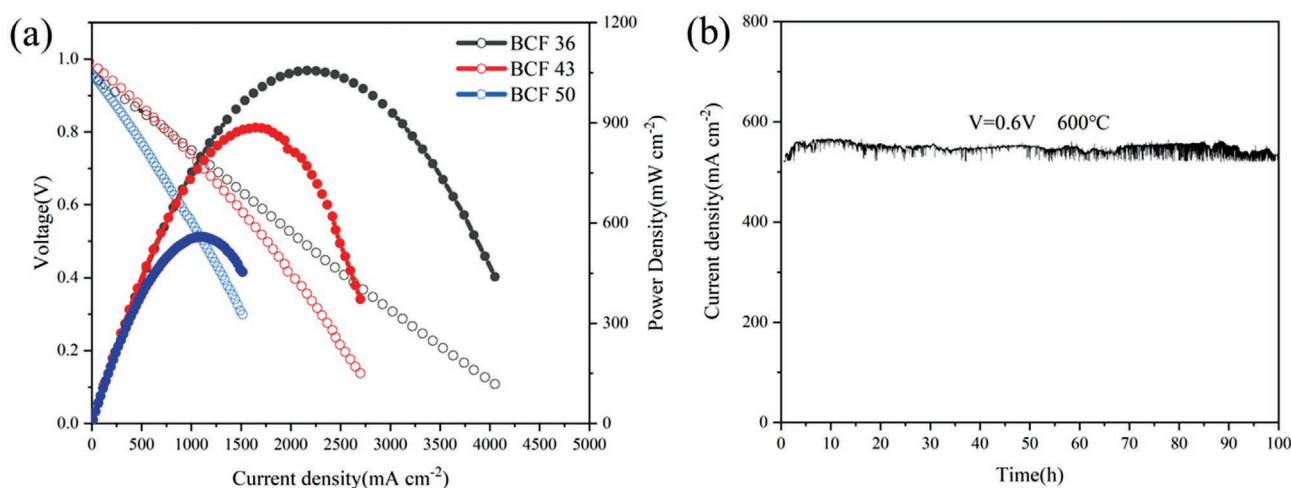


Figure 3. a) PVI curves of the single cells tested at 700 °C using BCF36, BCF43, and BCF50 cathodes and b) Operation stability test of a fuel cell with BCF36 cathode under a constant voltage of 0.6 V at 600 °C.

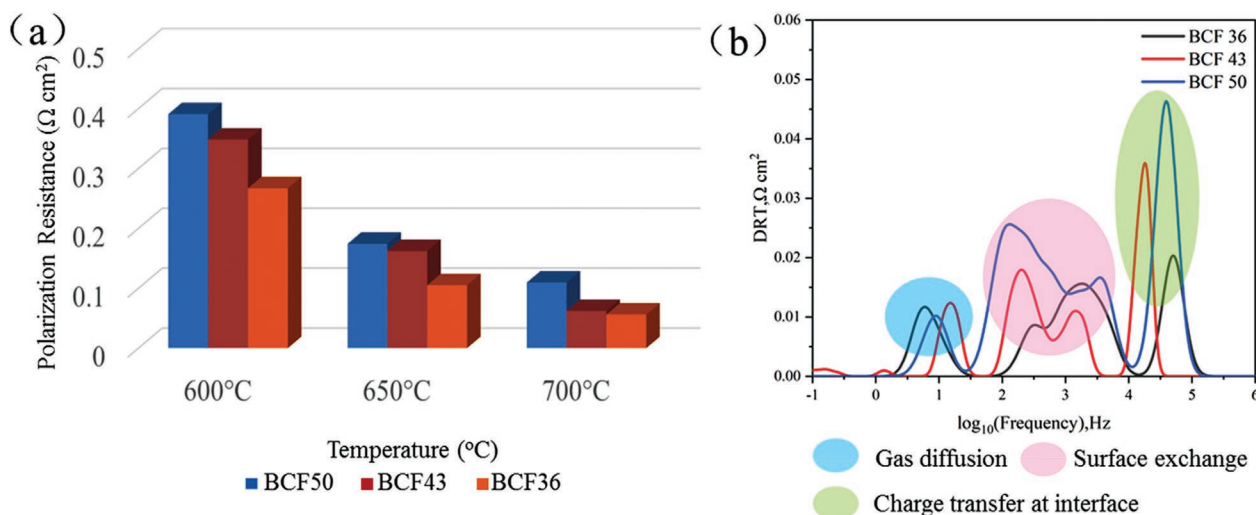


Figure 4. a) Comparison of the R_p values for BCF36, BCF43, and BCF50 cathodes at 600–700 °C, b) DRT analysis of the EIS data of the BCF36, BCF43, and BCF50 cathodes measured at 700 °C.

From the results of DRT analysis shown in Figure 4b, there exist several peaks denoted as high frequency (HF), intermediate frequency (IF), and low frequency (LF), respectively, corresponding to some key reaction steps involved in the cathode.^[34,36] The LF peaks of the different cathode compositions have no perceptible difference, indicating that the gas diffusion processes play insignificant role in the cathode reaction.^[37] The difference of IF range peaks associated with surface exchange as well as ion diffusion process illustrates that the ion diffusion of oxygen ion and proton plays a significant effect on the best performance of BCF36.^[38,39] In addition, the difference of HF peaks corresponding to charge transfer at interface^[40] also has an obvious influence on the cathode polarization reaction processes. Considering that the content of electron-conducting CP phase in BCF36 is significantly higher than the other two compositions, BCF36 is undoubtedly more conducive to charge transfer on the basis of electronic conductivity values. According to theoretical reaction processes, protons react

with oxygen ions at the triple phase boundaries (TPBs) on the cathode surface (Figure S12, Supporting Information). Notably, protons and oxygen ions can travel within the bulk of the composite cathode that will extend the TPB to the entire cathode surfaces by adjusting the assembled dual-phase composition to optimize intrinsic triple conducting behavior. Accordingly, the enhancement of TPB could help promote ion diffusion and reduce polarization resistance.

A simple spray-coating method is used to modify the BCF36 cathode microstructure. The spray-coated BCF36 particles have much smaller size compared to that of the screen printed cathode (Figure S13, Supporting Information). Particles with smaller size have uniform distribution and larger specific surface area is vital for the ORR activity. For single cells using spray-coated BCF36 cathode, the maximum power density reaches 1525 mW cm^{-2} while the R_p is 0.057 $\Omega \text{ cm}^2$ at 700 °C that can be seen in Figure 5. To achieve high ORR activity and cell performance for H-SOFCs, cobalt-containing cathodes have

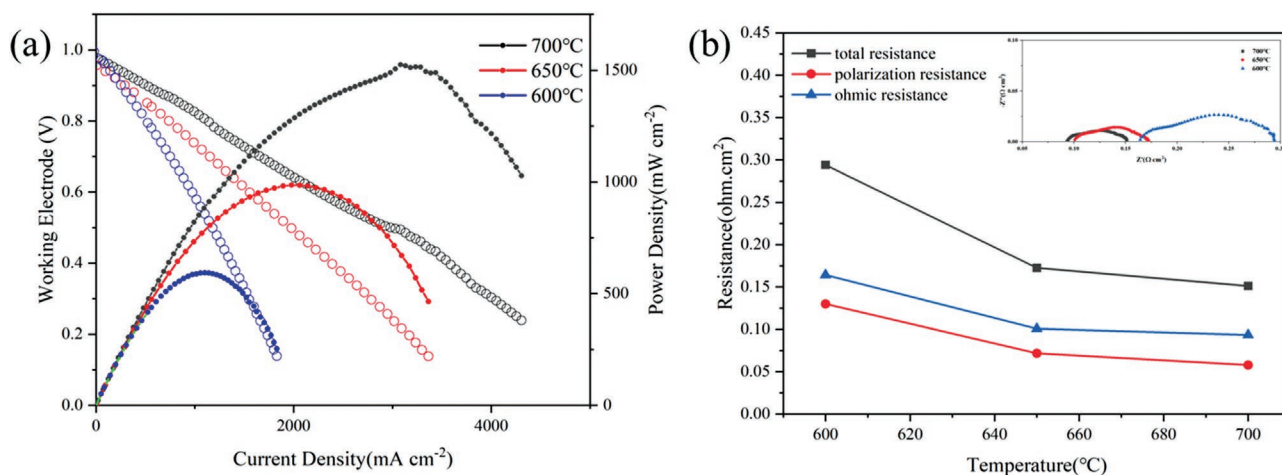


Figure 5. a) PVI curves of the single cells using BCF36 cathode by spraying, and b) Comparison of the R_t , R_p , and R_o values for BCF36 cathode by spraying at 600–700 °C.

Table 1. Performance comparison of proton-conducting SOFCs reported in the literature and in this study with different cathode materials measured at 700 °C.

Cathode materials	Electrolyte materials	Polarization resistance [$\Omega \text{ cm}^{-2}$]	Maximum power density [mW cm^{-2}]	Reference
BCF	BZCY	0.17	395	[21]
BSF-SDC	BZCY	0.044	696	[43]
SSFC-SDC	BZCYYb	0.138	505	[44]
BCP	BZCY	0.16	378	[45]
LSF	BZCY	0.14	377	[46]
PSCF-SDC	BZCY3	0.07	546	[47]
NBFNi10	BZCY	0.15	490	[48]
BCFB	BZCY	0.098	736	[49]
PDC-BCC-SBCC-CuO	BZCY	0.037	1000	[41]
LNO-LNF	BZCY	0.048	969	[42]
LSF-BZCY	BCZY	0.08	838	[50]
LNO, LNF nanofibers.	BZCY	0.128	551	[51]
BFSBi0.3	BZCY	0.032	1277	[14]
LSFCu	SDC	0.306	291	[52]
NBFM10	BZCY	0.06	453	[53]
LaSFM	SDC	0.211	269	[54]
BCF 36	BZCY	0.060	1056	This work
BCF 36 (spray coating)	BZCY	0.057	1525	This work

BZCY: $\text{BaZr}_{0.3}\text{Ce}_{0.7}\text{Y}_{0.2}\text{O}_{3-\delta}$; BZCY3: $\text{BaZr}_{0.3}\text{Ce}_{0.5}\text{Y}_{0.2}\text{O}_{3-\delta}$; BZCYYb: $\text{BaZr}_{0.1}\text{Ce}_{0.7}\text{Y}_{0.1}\text{Yb}_{0.1}\text{O}_{3-\delta}$; SDC: $\text{Sm}_{0.2}\text{Ce}_{0.8}\text{O}_{1.9}$; BCF: $\text{BaCe}_{0.5}\text{Fe}_{0.5}\text{O}_{3-\delta}$; BSF: $\text{Ba}_{0.5}\text{Sr}_{0.5}\text{FeO}_{3-\delta}$; LNO: $\text{La}_2\text{NiO}_{4+\delta}$; SSFC: $\text{Sm}_{0.5}\text{Sr}_{0.5}\text{Fe}_{0.8}\text{Cu}_{0.2}\text{O}_{3-\delta}$; BCP: $\text{BaCe}_{0.6}\text{Pr}_{0.4}\text{O}_{3-\delta}$; LSF: $\text{La}_{0.7}\text{Sr}_{0.3}\text{Fe}_{0.8}\text{O}_{3-\delta}$; PSCF: $\text{Pr}_{0.6}\text{Sr}_{0.4}\text{Cu}_{0.2}\text{Fe}_{0.8}\text{O}_{3-\delta}$; NBFN: $\text{Nd}_{0.5}\text{Ba}_{0.5}\text{Fe}_{0.9}\text{Ni}_{0.1}\text{O}_{3-\delta}$; BCFBi: $\text{BaCe}_{0.5}\text{Fe}_{0.3}\text{Bi}_{0.2}\text{O}_{3-\delta}$; PDC-BCC-SBCC: $\text{Ce}_{1-x}\text{Pr}_x\text{O}_{2-\delta}-\text{Ba}_2\text{CeCu}_3\text{O}_{7.4}-\text{Sm}_2\text{Ba}_{1.33}\text{Ce}_{0.67}\text{Cu}_3\text{O}_9$; LNF: $\text{LaNi}_{0.6}\text{Fe}_{0.4}\text{O}_{3-\delta}$; LZNO: $\text{La}_2\text{NiO}_{4+\delta}$; BFSBi0.3: $\text{BaFe}_{0.5}\text{Sn}_{0.2}\text{Bi}_{0.3}\text{O}_{3-\delta}$; LSFCu: $\text{La}_{0.6}\text{Sr}_{0.4}\text{Fe}_{0.8}\text{Cu}_{0.2}\text{O}_{3-\delta}$; NBFM10: $\text{NdBaFe}_{1.9}\text{Mn}_{0.1}\text{O}_{5+\delta}$; LaSFM: $\text{La}_{0.5}\text{Sr}_{0.5}\text{Fe}_{0.9}\text{Mo}_{0.1}\text{O}_{3-\delta}$; BCF 36: $\text{BaCe}_{0.36}\text{Fe}_{0.64}\text{O}_{3-\delta}$

been perceived as indispensable though many problems exist. Here, we provide a novel approach to design high-performing cobalt-free cathodes by tuning the cathode phase composition to improve the effect of synergistic integration and intrinsic triple conductivity. To highlight the superior property of the BCF samples, **Table 1** summarizes the performance of various cathodes of H-SOFCs reported in the literature. It can be seen that BCF36 cathode shows an excellent cell performance that is higher than most of other traditional cathodes, particularly cobalt-free cathodes, suggesting that self-assembled dynamic double phases would be an effective route to develop candidate cathodes for H-SOFCs. Moreover, the corresponding R_p values are 0.057, 0.073, and $0.131 \Omega \text{ cm}^2$ at 700, 650, and 600 °C, respectively. The activation energy (E_a) of spray-coated BCF36 calculated by the Arrhenius equation from the electrochemical impedance spectroscopy (EIS) is $\approx 0.61 \text{ eV}$. Though the R_p of BCF36 is a little higher than some cobalt-free cathodes, the E_a is relatively lower, compared to the E_a values of 1.31 eV for PDC-BCC-SBCC-CuO,^[41] 0.84 eV for BFSBi0.3^[14] and 1.43 eV for LNO-LNF,^[42] showing great potential to be applied at intermediate temperatures.

3. Conclusion

Composite phases where OP provides proton conductivity and CP supports mixed conductivity of oxygen ions and electrons

were self-assembled for BCF series cathodes. By tailoring the Ce/Fe amounts, the compositions changed according to the XRD refinement results and thus the intrinsic triple conductivity was modified. The ECR and electrochemical performance results revealed that BCF36 displayed the highest ORR activity and cell performance. Through microstructural optimization, single cells with BCF36 cathode possessed an unprecedented maximum power density of 1525 mW cm^{-2} at 700 °C compared with other cobalt-free cathodes for H-SOFCs. The in situ optimization of cathode composition enabled high ORR activity through adjusting triple conductivity and synergistic integration of the two phases, providing a promising approach to develop high-performance cathode for intermediate-temperature SOFCs.

4. Experimental Section

$\text{BaCe}_x\text{Fe}_{1-x}\text{O}_{3-\delta}$ ($x = 0.36, 0.43, \text{ and } 0.50$) powders were synthesized using a conventional combustion method via a citric acid sol-gel process.^[11] The precursors used in the powder preparation were BaCO_3 , $\text{Ce}(\text{NO}_3)_3 \cdot 6\text{H}_2\text{O}$, and $\text{Fe}(\text{NO}_3)_3 \cdot 9\text{H}_2\text{O}$. Proper amounts of raw materials were established as the stoichiometric ratio of the formula of the above powders. First, precursors with the appropriate amount were dissolved into dilute nitric acid solution while citric acid was added as complexing agents. The molar ratio of citric acid/total metal ions was controlled at 1.5. After that, the pH of the solution was adjusted to 7 using ammonia and a transparent solution was obtained. A solid gel was subsequently

obtained after continuously stirring at 80 °C for 6 h, which was self-ignited and combusted to form precursor powders, followed by calcination at 1000 °C for 3 h. BZCY powders were prepared via the same method above.

The crystalline phase and structure parameters of the prepared $\text{BaCe}_x\text{Fe}_{1-x}\text{O}_{3-\delta}$ powders were identified by X-ray diffraction (XRD, X'Pert3Powder) using CuK α radiation. The crystal structure and elemental distribution of the synthesized BCF36 was characterized using high resolution transmission electron microscope (HRTEM, JEM-2100F, JEOL, Japan). Cell microstructure was characterized by scanning electron microscope (SEM, Nova NanoSEM 450).

The porous anode substrate was pressed under 250 MPa using the mixture of BZCY, NiO, and starches at a weight ratio of 40:60:20 and then the loose BZCY powders were co-pressed on the anode substrate. In order to obtain a dense BZCY electrolyte, the half-cell was subsequently sintered at 1300 °C for 5 h. The cathode slurry of $\text{BaCe}_x\text{Fe}_{1-x}\text{O}_{3-\delta}$ was obtained by mixing $\text{BaCe}_x\text{Fe}_{1-x}\text{O}_{3-\delta}$ powders with appropriate amount of terpineol and ethylcellulose, which serves as the binder. The cathode slurry was screen printed on the electrolyte side of the half-cells and heat-treated at 1000 °C for 3 h. The electrode active area was 0.237 cm² and Ag paste was applied as current collector. Single cells with $\text{BaCe}_x\text{Fe}_{1-x}\text{O}_{3-\delta}$ ($x = 0.36, 0.43, \text{ and } 0.50$) cathode were named as BCF36, BCF43, and BCF50, respectively. In order to observe the influence of cathode microstructure on the cell performance, BCF36 powders were mixed with ethanol to form cathode slurry and then spray coated on the electrolyte. After drying, the assembled single cells were also heat-treated at 1000 °C for 3 h.

The surface exchange kinetics of BCF series cathodes were evaluated through electrical conductivity relaxation (ECR) measurement. Dense BCF bar samples were obtained by pressing the BCF powders at 300 MPa and sintering at 1250 °C for 5 h, achieving a relative density > 95%. Gas switching between gas mixture with $\text{N}_2:\text{O}_2 = 1:1$ and air at the same flow rate of $\approx 50 \text{ mL min}^{-1}$ was performed using a 4-way valve connected to the inlet line. The electrochemical performance of single cells was measured using an Admiral electrochemical workstation from 600 to 700 °C with wet H_2 ($\approx 3\% \text{H}_2\text{O}$) as fuel at a flow rate of 25 mL min⁻¹ and ambient air as oxidant.

Supporting Information

Supporting Information is available from the Wiley Online Library or from the author.

Acknowledgements

This work was supported by the National Natural Science Foundation of China (Grant Nos. 11875164), Joint Open Fund of Jiangsu Collaborative Innovation Center for Ecological Building Material and Environmental Protection Equipments, and Key Laboratory for Advanced Technology in Environmental Protection of Jiangsu Province (Grant No. 114269115), Natural Science Foundation of the Higher Education Institutions of Jiangsu Province (No. 18KJA430017) and the USA National Science Foundation (1832809).

Conflict of Interest

The authors declare no conflict of interest.

Data Availability Statement

The data that support the findings of this study are available from the corresponding author upon reasonable request.

Keywords

catalytic activity, composite cathodes, relaxation time, solid oxide fuel cells

Received: August 21, 2022

Revised: September 15, 2022

Published online:

- [1] L. Bi, S. P. Shafi, E. H. Da'as, E. Traversa, *Small* **2018**, *14*, 1801231.
- [2] L. Lei, Z. Tao, X. Wang, J. P. Lemmon, F. Chen, *J. Mater. Chem. A* **2017**, *5*, 22945.
- [3] J. Ma, Z. Tao, H. Kou, M. Fronzi, L. Bi, *Ceram. Int.* **2020**, *46*, 4000.
- [4] Y. Niu, Y. Zhou, W. Lv, Y. Chen, Y. Zhang, W. Zhang, Z. Luo, N. Kane, Y. Ding, L. Soule, Y. Liu, W. He, M. Liu, *Adv. Funct. Mater.* **2021**, *31*, 2100034.
- [5] L. Bi, S. Boulfrad, E. Traversa, *Chem. Soc. Rev.* **2014**, *43*, 8255.
- [6] C. Zuo, S. Zha, M. Liu, M. Hatano, M. Uchiyama, *Adv. Mater.* **2006**, *18*, 3318.
- [7] E. Fabbri, D. Pergolesi, E. Traversa, *Sci. Technol. Adv. Mater.* **2010**, *11*, 044301.
- [8] X. Kuai, G. Yang, Y. Chen, H. Sun, J. Dai, Y. Song, R. Ran, W. Wang, W. Zhou, Z. Shao, *Adv. Energy Mater.* **2019**, *9*, 1902384.
- [9] Y. Zhang, B. Yu, S. Lü, X. Meng, X. Zhao, Y. Ji, Y. Wang, C. Fu, X. Liu, X. Li, Y. Sui, J. Lang, J. Yang, *Electrochim. Acta* **2014**, *134*, 107.
- [10] Z. Tao, Y.-M. Jjiang, L. Lei, F. Chen, *Int. J. Hydrogen Energy* **2019**, *44*, 23539.
- [11] Z. Tao, M. Fu, Y. Liu, Y. Gao, H. Tong, W. Hu, L. Lei, L. Bi, *Int. J. Hydrogen Energy* **2022**, *47*, 1947.
- [12] E. Fabbri, L. Bi, D. Pergolesi, E. Traversa, *Energy Environ. Sci.* **2011**, *4*, 4984.
- [13] B. Lin, S. Zhang, L. Zhang, L. Bi, H. Ding, X. Liu, J. Gao, G. Meng, *J. Power Sources* **2008**, *177*, 330.
- [14] Y. Xia, Z. Jin, H. Wang, Z. Gong, H. Lv, R. Peng, W. Liu, L. Bi, *J. Mater. Chem. A* **2019**, *7*, 16136.
- [15] J. Kim, S. Sengodan, G. Kwon, D. Ding, J. Shin, M. Liu, G. Kim, *ChemSusChem* **2014**, *7*, 2811.
- [16] Y. S. Song, Y. B. Chen, W. Wang, C. Zhou, Y. J. Zhong, G. M. Yang, W. Zhou, M. L. Liu, Z. P. Shao, *Joule* **2019**, *3*, 2842.
- [17] D. Zou, Y. Yi, Y. Song, D. Guan, M. Xu, R. Ran, W. Wang, W. Zhou, Z. Shao, *J. Mater. Chem. A* **2022**, *10*, 5381.
- [18] K. Wei, N. Li, Y. Wu, W. Song, X. Wang, L. Guo, M. Khan, S. Wang, F. Zhou, Y. Ling, *Ceram. Int.* **2019**, *45*, 18583.
- [19] M. Fu, K. Li, Y. yang, Q. Zeng, L. Zeng, Z. Tao, *Sep. Puri. Technol.* **2022**, *287*, 120581.
- [20] Z. Tao, L. Bi, L. Yan, W. Sun, Z. Zhu, R. Peng, W. Liu, *Electrochem. Commun.* **2009**, *11*, 688.
- [21] Z. Tao, L. Bi, Z. Zhu, W. Liu, *J. Power Sources* **2009**, *194*, 801.
- [22] G. Li, Y. Zhang, Y. Ling, B. He, J. Xu, L. Zhao, *Int. J. Hydrogen Energy* **2016**, *41*, 5074.
- [23] X. Zhu, Y. Cong, W. Yang, *J. Membr. Sci.* **2006**, *283*, 158.
- [24] M. Zhu, Z. Cai, T. Xia, Q. Li, L. Huo, H. Zhao, *Int. J. Hydrogen Energy* **2016**, *41*, 4784.
- [25] G. C. Mather, D. Muñoz-Gil, J. Zamudio-García, J. M. Porras-Vázquez, D. Marrero-López, D. Pérez-Coll, *Appl. Sci.* **2021**, *11*, 5363.
- [26] J. F. Shin, W. Xu, M. Zanella, K. Dawson, S. N. Savvin, J. B. Claridge, M. J. Rosseinsky, *Nat. Energy* **2017**, *2*, 16214.
- [27] K. Xu, H. Zhang, Y. Xu, F. He, Y. Zhou, Y. Pan, J. Ma, B. Zhao, W. Yuan, Y. Chen, M. Liu, *Adv. Funct. Mater.* **2022**, *32*, 2110998.
- [28] C. Zhou, J. Sunarso, Y. Song, J. Dai, J. Zhang, B. Gu, W. Zhou, Z. Shao, *J. Mater. Chem. A* **2019**, *7*, 13265.
- [29] Y. Wang, B. Hu, Z. Zhu, H. J. M. Bouwmeester, C. Xia, *J. Mater. Chem. A* **2014**, *2*, 136.

- [30] L. Lei, Z. Tao, T. Hong, X. Wang, F. Chen, *J. Power Sources* **2018**, 389, 1.
- [31] D. Han, K. Shinoda, S. Sato, M. Majima, T. Uda, *J. Mater. Chem. A* **2015**, 3, 1243.
- [32] D. Wang, Y. Xia, H. Lv, L. Miao, L. Bi, W. Liu, *Int. J. Hydrogen Energy* **2020**, 45, 31017.
- [33] L. Lei, J. Zhang, R. Guan, J. Liu, F. Chen, Z. Tao, *Energy Convers. Manag.* **2020**, 218, 113044.
- [34] N. Shi, F. Su, D. Huan, Y. Xie, J. Lin, W. Tan, R. Peng, C. Xia, C. Chen, Y. Lu, *J. Mater. Chem. A* **2017**, 5, 19664.
- [35] Y. Zhang, Y. Chen, F. Chen, *J. Power Sources* **2015**, 277, 277.
- [36] D.-K. Lim, H.-N. Im, B. Singh, S.-J. Song, *J. Electrochem. Soc.* **2015**, 162, F547.
- [37] Y. Chen, Y. Choi, S. Yoo, Y. Ding, R. Yan, K. Pei, C. Qu, L. Zhang, I. Chang, B. Zhao, Y. Zhang, H. Chen, Y. Chen, C. Yang, B. deGlee, R. Murphy, J. Liu, M. Liu, *Joule* **2018**, 2, 938.
- [38] X. Wang, Z. Ma, T. Zhang, J. Kang, X. Ou, P. Feng, S. Wang, F. Zhou, Y. Ling, *ACS Appl. Mater. Interfaces* **2018**, 10, 35047.
- [39] B. Liu, H. Muroyama, T. Matsui, K. Tomida, T. Kabata, K. Eguchi, *J. Electrochem. Soc.* **2010**, 157, B1858.
- [40] R. Barfod, M. Mogensen, T. Klemensø, A. Hagen, Y.-L. Liu, P. Vang Hendriksen, *J. Electrochem. Soc.* **2007**, 154, B371.
- [41] J. Hou, L. Miao, J. Hui, L. Bi, W. Liu, J. T. S. Irvine, *J. Mater. Chem. A* **2018**, 6, 10411.
- [42] H. Tang, Z. Gong, Y. Wu, Z. Jin, W. Liu, *Int. J. Hydrogen Energy* **2018**, 43, 19749.
- [43] W. Sun, Z. Shi, S. Fang, L. Yan, Z. Zhu, W. Liu, *Int. J. Hydrogen Energy* **2010**, 35, 7925.
- [44] Y. Ling, J. Yu, B. Lin, X. Zhang, L. Zhao, X. Liu, *J. Power Sources* **2011**, 196, 2631.
- [45] Z. Tao, G. Hou, N. Xu, X. Chen, Q. Zhang, *Fuel Cells* **2014**, 14, 135.
- [46] Z. Tao, B. Wang, G. Hou, N. Xu, *Int. J. Hydrogen Energy* **2014**, 39, 16020.
- [47] Z. Gong, J. Hou, Z. Wang, J. Cao, J. Zhang, W. Liu, *Electrochim. Acta.* **2015**, 178, 60.
- [48] H. Shi, Z. Ding, G. Ma, *Fuel Cells* **2016**, 16, 258.
- [49] D. Shan, Z. Gong, Y. Wu, L. Miao, K. Dong, W. Liu, *Ceram. Int.* **2017**, 43, 3660.
- [50] X. Xu, L. Bi, X. S. Zhao, *J. Membr. Sci.* **2018**, 558, 17.
- [51] H. Tang, Z. Jin, Y. Wu, W. Liu, L. Bi, *Electrochem. Commun.* **2019**, 100, 108.
- [52] Q. Q. Zhou, L. Xu, Y. Guo, D. Jia, Y. Li, W. C. J. Wei, *Int. J. Hydrogen Energy* **2012**, 37, 11963.
- [53] X. Mao, T. Yu, G. Ma, *J. Alloys Compd.* **2015**, 637, 286.
- [54] M. Wu, H. Cai, F. Jin, N. Sun, J. Xu, L. Zhang, X. Han, S. Wang, X. Su, W. Long, L. Wang, L. Zhang, *J. Eur. Ceram. Soc.* **2021**, 41, 2682.